Mechanics of Materials 101 (2016) 93–101

Contents lists available at ScienceDirect

Mechanics of Materials

journal homepage: www.elsevier.com/locate/mechmat

Evaluation of stresses at the macro level based on computational micromechanics under finite strains

Néstor Darío Barulich[a,b], Luis Augusto Godoy[a,c,*], Patricia Mónica Dardati[b]

[a] Instituto de Estudios Avanzados en Ingeniería y Tecnología, IDIT UNC-CONICET, Ciudad Universitaria, Av. Vélez Sarsfield 1611, , X5016GCA, Córdoba, Argentina
[b] Universidad Tecnológica Nacional, Facultad Regional Córdoba, Maestro M. López esq. Cruz Roja Argentina, X5016ZAA, Córdoba, Argentina
[c] Universidad Nacional de Córdoba, FCEFyN, Ciudad Universitaria, Avda. Vélez Sarsfield 1611, X5016GCA, Córdoba, Argentina

ARTICLE INFO

Article history:
Received 9 March 2016
Revised 27 May 2016
Available online 20 July 2016

Keywords:
Fiber-reinforced composites
Finite elements
Finite strains
Homogenization
Micromechanics

ABSTRACT

A post-processing methodology to evaluate stresses at the macro level is presented. The methodology involves homogenization of a Representative Volume Element (RVE) or Unit Cell at the micro level by means of control nodes, with the consequence that numerical integration in the domain is not needed. This can be employed in cases of infinitesimal or finite strains; elastic, hyper-elastic or elastic-plastic materials under quasi-static processes. The paper shows that evaluation of stresses or material properties can be done in a RVE of simple shape, such as a prism, or in a RVE of complex shape, such as a truncated octahedron, using the proposed methodology. Use of the methodology is illustrated for cases under various conditions, for which comparison with independent results shows excellent agreement.

1. Introduction

Modeling of heterogeneous materials in terms of their microstructural characteristics, including volume fraction of each constituent, type and shape of inclusions, internal defects, is carried out at present by means of micro-mechanics (Nemat-Nasser and Hori, 1999). At least two scales are considered: a microscopic scale, in which details of the microstructure are represented, and a macroscopic scale in which an homogeneous material is considered to represent the heterogeneous properties by means of an equivalence. The region of heterogeneous material at the micro level necessary to capture the macroscopic behavior is taken as a Representative Volume Element (RVE) or a Unit Cell (UC), and analytical or numerical procedures are employed next to model the behavior at a macro level.

Computational Micro Mechanics (CMM) takes advantage of computational procedures to represent details of behavior which would not be accessible by analytical techniques (Zohdi and Wriggers, 2008); however, the cost of employing CMM in two-scale problems is the need to employ large computer resources, so that there are motivations to reduce computational cost whenever possible. Homogenization is a key ingredient in CMM modeling and improvements in this part of the process may yield considerable improvements in performance.

Homogenization is commonly employed in two steps of the modeling process: (a) the approximate solution of the boundary value problem by means of numerical methods; and (b) the post-processing of results to evaluate variables of interest at the macro level, such as stresses, elastic properties, etc. This work focuses on the second stage, i. e. the post-processing homogenization.

Homogenization post-processing may be oriented to compute stresses at the macro level based on micromechanics information. For small strains, the usual definition of macro stress is given by Nemat-Nasser and Hori (1999)

$$\boldsymbol{\sigma} = \frac{1}{V}\int_V \sigma^m \, dV \tag{1}$$

where $\boldsymbol{\sigma}$ is the stress at the macro level; $\boldsymbol{\sigma}^m$ is the Cauchy stress in the RVE; and V is the volume of the RVE. Index m on top of a variable indicates that it belongs to the microscopic scale. A similar expression is employed for large strains, but integration is performed on the current configuration rather than the initial configuration, as discussed in de Souza-Neto and Feijóo (2008).

Within the context of small strain problems, the definition of the macroscopic stress emerges, after Gauss theorem is used, in the form

$$\boldsymbol{\sigma} = \frac{1}{V}\int_{\partial V} \mathbf{X} \otimes \mathbf{t} \, dS \tag{2}$$

where ∂V is the boundary of the RVE; $\mathbf{X}$ is the coordinate of a point at ∂V; $\mathbf{t}$ is the traction vector in ∂V. The Cartesian components of the tensor product between two vectors $\mathbf{a}$ and $\mathbf{b}$ are

* Corresponding author.
E-mail address: luis.godoy@unc.edu.ar (L.A. Godoy).

http://dx.doi.org/10.1016/j.mechmat.2016.07.006
0167-6636/

written as

$$[\mathbf{a}\otimes\mathbf{b}]_{ij}=a_i b_j \tag{3}$$

Numerical implementation of Eq. (1) may be performed for infinitesimal strains, as explained by Barbero (2013), or for finite strains, as discussed by Abadi (2010) and Guo et al. (2014), among others.

Zahr-Viñuela and Pérez-Castellanos (2011) implemented two homogenization processes in the evaluation of macro stresses with finite strains, identified by the authors as "external measure" and "internal measure". Macroscopic stresses are evaluated in the first case by means of a force which is applied to a control node divided by the actual cross area. In the internal measure, the integral in Eq. (1) is approximated as

$$\sigma_{ij}=\frac{1}{v}\sum_{k=1}^{N}\sigma_{ij}^{k}v_k \tag{4}$$

where $\sigma^k{}_{ij}$ is the ij component of the microscopic Cauchy tensor at the k Gauss point in the element used in the discretization of the RVE; v_k is the weight factor for numerical integration (in terms of volume in the current configuration associated with Gauss point k) for a mesh with N Gauss points; and v is the volume in the current configuration of the RVE. All these variables depend on time.

An alternative formulation for finite strains has been presented by Dijk (2015) for computational homogenization based on virtual work and the Hill-Mandel Principle for periodic boundary conditions. Dijk employs Lagrange multipliers so that the stress measures at macro level become conjugate forces of the macro strains, or vice versa; this formulations is limited to RVE with periodic boundaries

The computation of macro stresses by means of a simple equation was reported by Li and Wongsto (2004), based on an energy equivalence between micro and macro scales (Hill-Mandel condition, see Nemat-Nasser and Hori, 1999). The studies in Li and Wongsto (2004) were applied to particle-reinforced composites, for RVE with shapes adequate to model different packaging configurations of particles. In the mid-1990s, Sun and Vaidya (1996) presented a similar idea but did not apply their methodology to complex shapes. In both Li and Wongsto (2004), and Sun and Vaidya (1996) the problem was formulated for infinitesimal strains.

A methodology for post-processing stresses is presented in this work for finite strains; this is abbreviated as PPM-FS (Post-Processing Methodology for Finite Strains) and should be applicable to linear as well as to nonlinear problems. The goal is to deal with UC problems with internal cracks in contact including material nonlinearity, i.e. plasticity or hyper-elasticity, and geometric nonlinearity. Complex RVE shapes are also of interest, such as a truncated octahedron.

Notice that economies in time and computational cost may be small with respect to the time required to solve the RVE; however, the present methodology avoids the complexities associated with numerical integration.

2. Post-processing methodology

2.1. Geometry of unit cells considered

Two types of UC shown in Fig. 1 are investigated in this work: A prism having a parallelogram with equal sides at the base; and the truncated octahedron. The latter case has been employed in the literature to represent particle-reinforced composites (Li and Wongsto, 2004), crystalline structures (Delannay et al., 2006), and open cell materials such as metal foam (Dharmasena and Wadley, 2002). In the present research both RVE geometries are used to model a composite material reinforced with unidirectional fibers.

Periodicity vectors, as described for example in Oller et al. (2005), are here employed to model the microstructure in a periodic material. Three periodicity vectors are used for a UC, as shown in Fig. 1: For the prismatic UC, these vectors are

$$\mathbf{P1}=lf\,\mathbf{i};\quad \mathbf{P2}=2b\,\mathbf{j};\quad \mathbf{P3}=2b\cos(\theta)\mathbf{j}+2b\sin(\theta)\mathbf{k} \tag{5}$$

where lf is the fiber length; and θ and b are shown in Fig. 2a. The relation of θ and b with Vf (fiber volume fraction) may be written as

$$b=Rf\sqrt{\frac{\pi}{4Vf\sin(\theta)}} \tag{6}$$

were Rf is the fiber radius. For the truncated octahedron, the periodicity vectors are

$$\mathbf{P1}=lf_o\mathbf{i};\quad \mathbf{P2}=\frac{lf_o}{3}\mathbf{i}+lf_o\sqrt{\frac{2}{3}}\mathbf{j}+\frac{\sqrt{2}}{3}lf_o\mathbf{k};$$

$$\mathbf{P3}=\frac{2}{3}lf_o\mathbf{i}+\frac{2\sqrt{2}}{3}lf_o\mathbf{k} \tag{7}$$

where lf_o is the fiber length, computed in terms of length le shown in Fig. 2

$$lf_o=\sqrt{6}\,le;\quad \text{with}\quad le=Rf\sqrt{\frac{\pi\sqrt{3}}{8Vf}} \tag{8}$$

2.2. Periodic boundary conditions under finite strains

Periodic Boundary Conditions (PBC) have been described in the literature on computational micro-mechanics, such as Guo et al. (2007, 2014) and Abadi (2010), and were used in this work to represent a periodic composite at finite strains. Following the nomenclature adopted in Zahr-Viñuela and Pérez-Castellanos (2011), two points in a microstructure are identified as "corresponding points" if the position of one of them may be obtained as the position of the other one plus a linear combination of the periodicity vectors using integer coefficients. To illustrate the concept, periodicity vectors $\mathbf{P_1}$ and $\mathbf{P_2}$ are shown in Fig. 3. The points in pairs: (C_0; C_1), (C_0; C_2) and (C_0; C_3) are corresponding points.

The boundary conditions are relations involving the forces and displacements at the boundary of the cell (Guo et al., 2007, 2014). If the traction vector at a boundary point and its corresponding boundary point are $\mathbf{t}^+$ y $\mathbf{t}^-$ respectively, then the following condition should be satisfied at all boundary pairs of points

$$\mathbf{t}^+=-\mathbf{t}^- \tag{9}$$

Assuming that the locations at a boundary point, in the actual configuration, are written as $\mathbf{x}^+$ and at its corresponding point as $\mathbf{x}^-$, then the condition

$$\mathbf{x}^+-\mathbf{x}^-=\mathbf{F}(\mathbf{X}^+-\mathbf{X}^-) \tag{10}$$

applies at all boundary points (Guo et al., 2014, Eq. (9)), where $\mathbf{X}^+$ and $\mathbf{X}^-$ are the locations of the points in the reference configuration; and $\mathbf{F}$ is the imposed macroscopic deformation gradient.

Eq. (10) is next written as a function of nodal displacements at the boundary in order to facilitate implementation in the general purpose finite element package ABAQUS (2009) by means of command termed *EQUATION. The deformation gradient can be written as

$$\mathbf{F}=\nabla\mathbf{U}+\mathbf{I} \tag{11}$$

where $\nabla\mathbf{U}$ is the macroscopic displacement gradient in the reference configuration; and $\mathbf{I}$ is the identity tensor. The components of operator ∇ are

$$[\nabla(\cdot)]_{ij}=\frac{\partial(\cdot)_i}{\partial X_j} \tag{12}$$

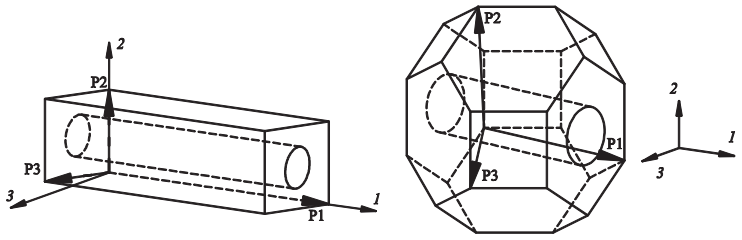

Fig. 1. Periodicity vectors in UC of a fiber reinforced composite: (a) Prismatic; (b) Truncated octahedron.

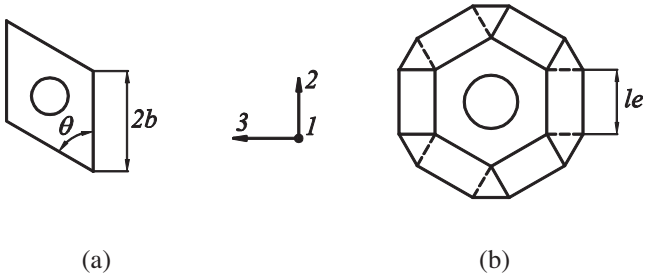

Fig. 2. Front view of a UC: (a) Prismatic; (b) Truncated octahedron.

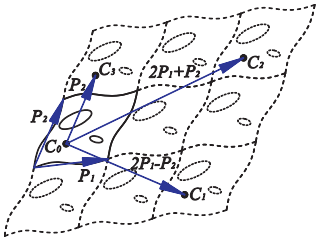

Fig. 3. Example of corresponding points in a periodic material.

Substitution of Eq. (11) into (10) yields

$$\mathbf{x}^+ - \mathbf{x}^- = \nabla\mathbf{U}(\mathbf{X}^+ - \mathbf{X}^-) + \mathbf{X}^+ - \mathbf{X}^- \tag{13}$$

Next, the displacement at a point is written as the difference between the current location minus the reference location,

$$\mathbf{u}^+ - \mathbf{u}^- = \nabla\mathbf{U}\,\mathbf{Pv} \tag{14}$$

where **Pv** is a periodicity vector (or a linear combination of them) which satisfies the condition

$$\mathbf{Pv} = \mathbf{X}^+ - \mathbf{X}^- \tag{15}$$

For a UC modeled by finite elements, it is only necessary to specify the conditions (14) for the boundary displacements. The antiperiodic conditions (9) for the boundary tractions are automatically satisfied because a displacement-based variational finite element formulation has been employed, as explained in Li and Wongsto (2004).

The conditions (14) were implemented in this work by means of multipoint linear constraints. From Eq. (14), the scalar equation holds

$$u_i{}^+ - u_i{}^- \; - \frac{1}{\alpha} w_i^1 Pv_x \; - \frac{1}{\alpha} w_i^2 Pv_y \; - \frac{1}{\alpha} w_i^3 Pv_z \; = 0 \tag{16}$$

where $i = 1, 2, 3$; Pv_x, Pv_y, and Pv_z are the **Pv** vector components; α is a unit factor, $\alpha = 1$ [length units] to homogenize units; $w_i{}^j$ are the displacement components in direction i of the additional node j that has been included as a control node. Three control nodes have been selected in this work, and a boundary condition is assigned to them in terms of the components of the macroscopic displacement gradient which is to be imposed on the UC:

$$w_i^j = \alpha[\nabla\mathbf{U}]_{ij} \tag{17}$$

Eqs. (17) and (16) include a unit factor α to avoid dimensional inconsistencies. Eq. (14) are thus implemented by use of Eq. (16) and boundary conditions (17), which are valid for any RVE or UC geometric configuration.

The identification of faces, edges, and vertices for a UC with the shape of a prism is shown in Fig. 4, and for a truncated octahedron in Fig. 5. A summary of the **Pv** vectors to be used with each pair of nodes on faces, edges, and vertices is given in Tables 1– 6 for the first and second degree of freedom (DOF) in Eq. (16).

Table 1
Pv vectors of different pairs of faces of the prismatic UC.

Faces		
1st DOF	2nd DOF	**Pv**
R	L	**P1**
S	I	**P2**
F	P	**P3**

Table 2
Pv vectors of different pairs of vertices of the prismatic UC.

Vertices		
1st DOF	2nd DOF	**Pv**
V2	V1	**P1**
V5	V1	**P2**
V3	V1	**P3**
V4	V1	**P1+P3**
V7	V1	**P2+P3**
V6	V1	**P1+P2**
V8	V1	**P1+P2+P3**

Table 3
Pv vectors of different pairs of edges of the prismatic UC.

Edges		
1st DOF	2nd DOF	**Pv**
E3	E1	**P2**
E11	E1	**P3**
E12	E1	**P2+P3**
E8	E5	**P1**
E7	E5	**P2**
E10	E5	**P1+P2**
E4	E2	**P1**
E6	E2	**P3**
E9	E2	**P1+P3**

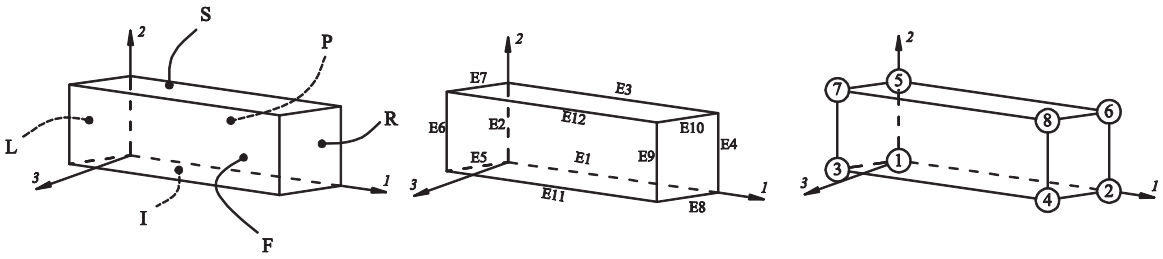

Fig. 4. Identifications of faces edges and vertices in a prismatic UC.

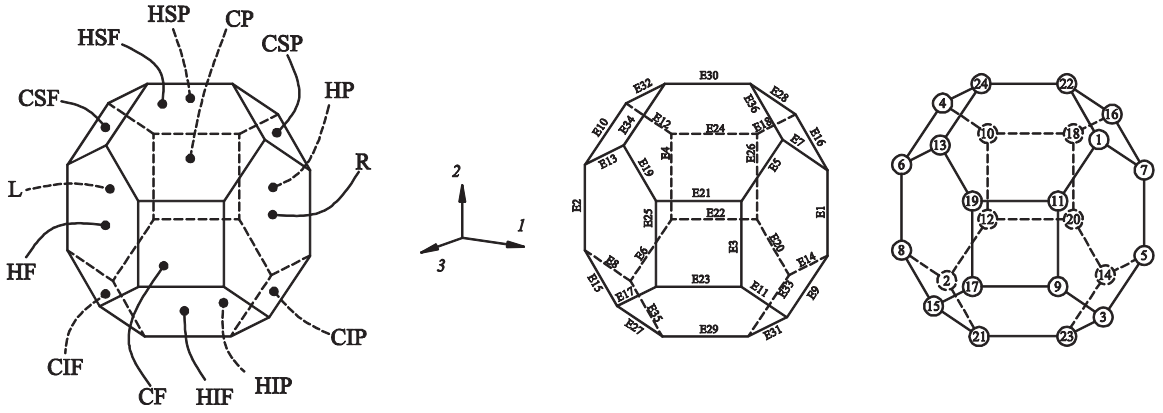

Fig. 5. Identifications of faces, edges, and vertices in a UC with shape of a truncated octahedron.

Table 4
Pv vectors of different pairs of faces for the truncated octahedron UC.

1st DOF	2nd DOF	**Pv**
R	L	**P1**
CF	CP	**P3**
HF	HP	**P3− P1**
CSF	CIP	**P2−P1**
HSF	HIP	**P2**
CSP	CIF	**P1+P2−P3**
HSP	HIF	**P2−P3**

Table 5
Pv vectors of different pairs of edges for the truncated octahedron UC.

1st DOF	2nd DOF	**Pv**	1st DOF	2nd DOF	**Pv**
E1	E4	**P1**	E18	E13	**P1 −P3**
E25	E4	**P3**	E31	E13	**P1 −P2**
E26	E2	**P1 −P3**	E14	E17	**P1 −P3**
E3	E2	**P1**	E32	E17	**P2 −P3**
E5	E10	**P1**	E16	E19	**P1 −P3**
E33	E10	**P1 −P2**	E35	E19	**−P2**
E9	E6	**P1**	E20	E15	**P1 −P3**
E34	E6	**P2**	E36	E15	**P1+P2 −P3**
E7	E12	**P1**	E21	E24	**P3**
E27	E12	**P3 − P2**	E29	E24	**P3 −P2**
E11	E8	**P1**	E23	E30	**P3 −P2**
E28	E8	**P1+P2 −P3**	E22	E30	**−P2**

Whenever periodicity is implemented by Eq. (16) and boundary conditions (17), there are three control nodes at which displacements can be imposed by Eq. (17) for a given deformation gradient **F**. Thus, at nodes in which displacements are specified there will be reactive forces which can be obtained from the finite element model. These forces and displacements will be employed in this work in the post-processing to achieve homogenization.

Table 6
Pv vectors of different pairs of vertices for the truncated octahedron UC.

1st DOF	2nd DOF	**Pv**	1st DOF	2nd DOF	**Pv**
V17	V12	**P3**	V7	V10	**P1**
V5	V12	**P1**	V19	V10	**P3**
V24	V12	**P2**	V21	V10	**P3 −P2**
V9	V8	**P1**	V3	V2	**P1**
V22	V8	**P1+P2 −P3**	V16	V2	**P1+P2−P3**
V20	V8	**P1 −P3**	V13	V2	**P2**
V11	V6	**P1**	V1	V4	**P1**
V23	V6	**P1 −P2**	V14	V4	**P1 −P2**
V18	V6	**P1 −P3**	V15	V4	**P3 −P2**

2.3. Evaluation of stresses at macro level

2.3.1. Internal mechanical power

Under a given strain state, a stress field is induced at a RVE. The stress power, or rate of internal mechanical work, identified as *Pint(t)*, is a scalar associated with the stress field acting on the RVE in the reference configuration V at time t. Following Holzapfel (2000), *Pint* is given by

$$Pint(t) = \int_V \mathbf{P}^m : \dot{\mathbf{F}}^m dV \tag{18}$$

where $\mathbf{P}^m$ is the first Piola-Kirchhoff tensor; and $\dot{\mathbf{F}}^m$ is the rate of deformation gradient **F**. Units of *Pint(t)* are work per time unit.

The first Piola-Kirchhoff tensor satisfies the condition

$$\mathbf{P} = J\sigma\left(\mathbf{F}^{-1}\right)^T \tag{19}$$

where $J = det(\mathbf{F})$ is the Jacobian of **F**. Next, consider

$$\dot{\mathbf{F}} = \nabla(\mathbf{Vel}(\mathbf{X}, t)) \tag{20}$$

Vel is the velocity and is written in terms of reference configuration **X** at a time t.

For a RVE, the Hill-Mandel condition may be written as de Souza-Neto and Feijóo (2008)

$$\mathbf{P} : \dot{\mathbf{F}} = \frac{1}{V}\int_V \mathbf{P}^m : \dot{\mathbf{F}}^m dV \tag{21}$$

where $\mathbf{P}^m$ and $\mathbf{P}$ are the first Piola-Kirchhoff tensor at the micro and the macro scales, respectively; $\dot{\mathbf{F}}^m$ and $\dot{\mathbf{F}}$ are the rates of deformation gradient again at micro and macro scales. Body force and inertia have not been included in this work, but these effects have been taken into account by de Souza-Neto et al. (2015).

Thus, the stress power results in

$$Pint(t) = V\ \mathbf{P} : \dot{\mathbf{F}} \tag{22}$$

For the specific case of simple shear in which $\mathbf{F}$ is given by

$$\mathbf{F}(t) = \begin{bmatrix} 1 & 0 & 0 \\ \gamma_f t & 1 & 0 \\ 0 & 0 & 1 \end{bmatrix} \tag{23}$$

for $0 \le t \le 1$ [sec], one has

$$Pint(t)_{shear} = V\ \sigma_{12}\ \gamma_f \tag{24}$$

Notice that in the case of shear, a tensor of simple shear needs to be used instead of a tensor of pure shear because the latter induces a stress power which would not be associated with a unique macroscopic stress.

In the case of uniaxial strain, a principal stretching λ_1 is applied in direction 1, whereas λ_2 and λ_3 are computed to obtain $\sigma_{22} = \sigma_{33} = 0$ through a deformation gradient

$$\mathbf{F}(t) = \begin{bmatrix} \lambda_1(t) & 0 & 0 \\ 0 & \lambda_2(t) & 0 \\ 0 & 0 & \lambda_3(t) \end{bmatrix} \tag{25}$$

where

$$\lambda_1(t) = 1 + (\lambda_{1F} - 1)t \tag{26}$$

for $0 \le t \le 1$ [sec], where λ_{1F} is the final principal stretching, the stress power reduces to

$$Pint(t)_{uniaxial} = V\ (\lambda_{1F} - 1)\lambda_2\ \lambda_3\ \sigma_{11} \tag{27}$$

Again, all variables in Eq. (27) depend on t, with the exception of V.

2.3.2. External mechanical power

If the kinetic energy change in the RVE is zero, then the problem may be classified as quasi-static, in which the variables may still be time-dependent. The energy balance results in

$$Pext(t) = Pint(t) \tag{28}$$

where $Pext(t)$ is the external mechanical power or rate of mechanical external work (see Holzapfel, 2000, Eq. 4.102). $Pext(t)$ is defined as the power due to external forces in a domain of volume V at time t.

In a finite element model of a RVE with control nodes, external work is only done through forces acting on such control nodes. Thus, the external power for each loading case considered is the product of the force (reaction) multiplied by the velocity in the direction of the force. For simple shear this is

$$Pext(t)_{shear} = \alpha R_{12}\ \gamma_f \tag{29}$$

where R_{12} is the force in direction 1 acting in control node 2; whereas

$$Pext(t)_{uniaxial} = \alpha R_{11}\ (\lambda_{1F} - 1) \tag{30}$$

holds for uniaxial strains, in which R_{11} is the force in direction 1 acting in control node 1.

2.3.3. Evaluation of macroscopic stresses

Consider the energy balance of Eq. (28) together with Eqs. (24) and (29) for simple shear; then the components of the Cauchy stress at the macro level become

$$\sigma_{12} = \frac{\alpha R_{12}}{V} \tag{31}$$

where σ_{12} is the Cauchy stress component at macro level.

For uniaxial strain, using Eqs. (28), (27) and (30), the Cauchy stress at macro level σ_{11} is

$$\sigma_{11} = \frac{\alpha R_{11}}{V\lambda_2\lambda_3} \tag{32}$$

As stated before, variables in Eqs. (31) and (32) depend on t, with the exception of V.

The homogenization procedure may be now summarized as follows: (i) displacements are first obtained in the RVE at time t, and reactions (either R_{11} or R_{12}) are identified at the control node. (ii) the principal macroscopic stretching λ_2 and λ_3 are computed as

$$\lambda_2(t) = 1 + w_2^2 \tag{33}$$

$$\lambda_3(t) = 1 + w_3^3 \tag{34}$$

where $w_2{}^2$ and $w_3{}^3$ are displacements of control nodes 2 and 3 in directions 2 and 3, respectively (see Eq. 16). (iii) depending on the case considered, Eq. (31) or (32) is used to obtain the Cauchy stress component at macro level.

The conditions to perform homogenization under simple shear in a direction different than that considered for Eq. (31) may be obtained by the same procedure and results in

$$\sigma_{13} = \frac{\alpha R_{13}}{V};\quad \sigma_{23} = \frac{\alpha R_{23}}{V} \tag{35}$$

for the shear components, whereas the normal components are given by

$$\sigma_{22} = \frac{\alpha R_{22}}{V\lambda_1\lambda_3};\quad \sigma_{33} = \frac{\alpha R_{33}}{V\lambda_1\lambda_2} \tag{36}$$

An important advantage of the present PPM-FS is that numerical integration need not be used, with the consequence that less complexity in implementation and less information and computer time are handled during the post-process. Because the method is based on mechanical energy balance in quasi-static problems, the range of application includes material or kinematic nonlinearities. Further, the methodology is not only appropriate for PBC but also for any boundary condition that satisfies Hill-Mandell condition and could be implemented by means of control nodes. In its present form, the proposed methodology can only tackle states of uniaxial stress and simple shear, which allow computation of effective tangent constitutive tensors associated to those stress states.

3. Results for UC under simple shear

To validate results of the present PPM-FS, several cases have been solved by means of a finite element implementation using ABAQUS (2009). Specifically, elements with linear interpolation were used because of their advantages in modeling plasticity and incompressible materials. Convergence was investigated in each case with up to approximately 200,000 elements in cases with plasticity.

3.1. Small strain problem

As an initial example, a case reported in the literature (examples 6.2 and 6.3 in Barbero, 2013) is solved under small strains. This consists in the evaluation of G_{12}, the in-plane shear modulus of a periodic composite reinforced with long carbon fibers in a

Table 7
Fiber and matrix properties from Barbero (2013).

	Carbon fiber AS4-D	Epoxy matrix 9310/9360[a] 23 °C
E [GPa]	241	3.12
ν	0.2	0.38

Table 8
Comparison for shear modulus G_{12}.

	Barbero (2013)	Present metodology
G_{12} [MPa]	2579	2583

polymer matrix. The UC adopted in Barbero (2013) is a rectangular parallelepiped in which fibers have an hexagonal configuration. Matrix and fiber properties (shown in Table 7) are assumed as linear elastic and isotropic, for a composite with 40% fiber volume fraction.

The gradient of displacement in the material description can be computed based on the macroscopic deformation gradient as (see Eq. 2.45 in Holzapfel, 2000)

$$\nabla \mathbf{U} = \mathbf{F} - \mathbf{I} \tag{37}$$

Under infinitesimal displacements, the gradient of displacements in the material description, Eq. (37), is approximately the same as in the actual or spacial description. Thus, the tensor of infinitesimal strain can be obtained as the symmetric part of Eq. (37), as indicated in Chandrasekharaiah and Debnath (2014) (Eq. 5.6.4)

$$\varepsilon = \frac{1}{2}\left(\nabla \mathbf{U} + \nabla \mathbf{U}^T\right) \tag{38}$$

The small strain tensor becomes

$$\varepsilon = \begin{bmatrix} 0 & 5x10^{-5} & 0 \\ 5x10^{-5} & 0 & 0 \\ 0 & 0 & 0 \end{bmatrix} \tag{39}$$

Rather than using the same geometry of the UC as in the original reference, in this case a truncated octahedron was employed to illustrate its use.

Finally, evaluation of the shear modulus G_{12}, is obtained by dividing Cauchy stress computed by Eq. (31) and the associated strain component for infinitesimal strains. Results of Table 8 show good agreement between the present results based on the truncated octahedron and those by Barbero.

3.2. Comparison with an analytical model for finite strains

To investigate the response of the proposed methodology under large shear strains, an analytical model due to Abadi (2010) for fiber and matrix of Neo-Hookean isotropic incompressible hyper-elastic material has been used for comparison. The strain energy density W of a Neo-Hookean isotropic incompressible hyper-elastic material is (see Holzapfel, 2000)

$$W(t) = C_{10}(I_1(t) - 3) \tag{40}$$

were C_{10} is a material parameter, and the first invariant of strain I_1 is given by

$$I_1(t) = \mathrm{tr}\left[\mathbf{F}(t)^T \mathbf{F}(t)\right] \tag{41}$$

If the material undergoes transverse or axial simple shear in a composite with hyper-elastic and incompressible properties ($J = 1$), W^C results in (see Abadi, 2010)

$$W^c(t) = C^c_{10}(I_1(t) - 3) \tag{42}$$

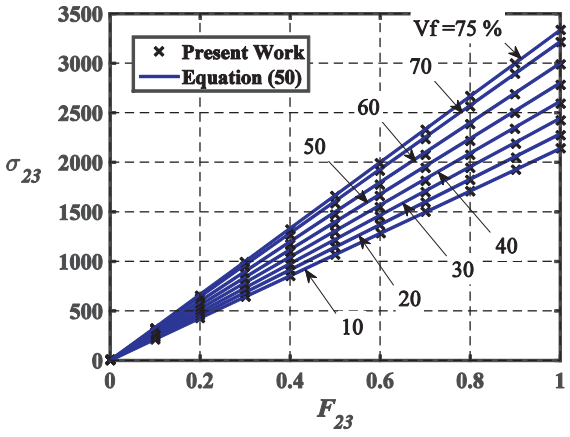

Fig. 6. Cauchy stress [MPa] for a hyper-elastic composite under transversal simple shear: Comparison between PPM-FS and analytic model of Abadi (2010).

where the material parameter is

$$C^c_{10} = \frac{(1+Vf)C^f_{10} + (1-Vf)C^m_{10}}{(1-Vf)C^f_{10} + (1+Vf)C^m_{10}} \tag{43}$$

and $C_{10}{}^f$ y $C_{10}{}^m$ are material parameters of fiber and matrix, respectively. The specific case of interest is a composite under simple transverse shear strain, with a deformation gradient given by

$$\mathbf{F}(t) = \begin{bmatrix} 1 & 0 & 0 \\ 0 & 1 & \gamma_f t \\ 0 & 0 & 1 \end{bmatrix} \tag{44}$$

The density W^C in Eq. (42), reduces to

$$W^c(t) = C^c_{10}\,\gamma_f^2\,t^2 \tag{45}$$

The time rate of W^C is

$$\frac{dW^c(t)}{dt} = 2C^c_{10}\gamma_f^2 t \tag{46}$$

The strain energy rate can be written in terms of stress and strain rate, i.e.

$$\frac{dW(t)}{dt} = \mathbf{P} : \dot{\mathbf{F}} \tag{47}$$

For the case of shear strain and considering Eq. (19), the strain energy rate becomes

$$\frac{dW(t)}{dt} = \sigma_{23}\gamma_f \tag{48}$$

Cauchy stress can now be obtained from Eqs. (46) and (48) in the form

$$\sigma_{23} = 2C^c_{10}\gamma_f t \tag{49}$$

Finally, Cauchy stress σ_{23} can be obtained as

$$\sigma_{23} = 2C^c_{10}F_{23} \tag{50}$$

To compare numerical results, consider a fiber reinforced composite in a square fiber arrangement (prismatic UC with $\theta = 90$ in Fig. 2a). A deformation gradient (44) is imposed and Eq. (35) is used to compute the stresses at the macro scale. Results of macro stress are compared in Fig. 6 under simple transverse shear under large strains: The present model predicts the same results as the analytical model.

3.3. Comparison with a numerically integrated model for finite strains

The present post-processing methodology has been applied to a composite with continuous fibers in hexagonal configuration

Table 9
Ogden material properties.

Matrix: Ogden	
μ_i [N/m^2]	α_i
6.3×10^5	1.3
0.012×10^5	5
-0.1×10^5	−2

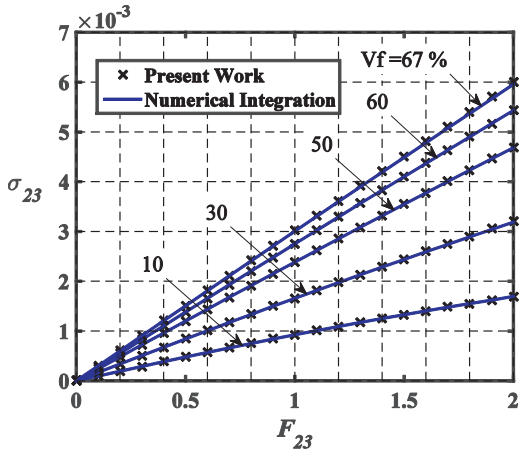

Fig. 7. Cauchy stress [GPa] for a hyper-elastic composite under transversal simple shear: Comparison between PPM-FS and numerical integration of Eq. (4).

(prismatic UC), having $0.1 \le Vf \le 0.67$. Isotropic hyper-elastic incompressible behavior is assumed for fiber and matrix, with Neo-Hookean model for the fibers (Eq. (40)) and Ogden model for the matrix (Eq. (51)).

$$W(t) = \sum_{i=1}^{N} \frac{2\mu_i}{\alpha_i^2}\left[\lambda_1^{\alpha_i} + \lambda_2^{\alpha_i} + \lambda_3^{\alpha_i} - 3\right] \tag{51}$$

where μ_i and α_i are material parameters; N is the number of terms used in the model; λ_i are the principal stretching of the deformation gradient acting in the material. The initial shear modulus for the assumed Neo-Hookean material is given by

$$\mu_0^f = 2C_{10} \tag{52}$$

For the Ogden material, the initial shear modulus is

$$\mu_0^m = \sum_{i=1}^{N} \mu_i \tag{53}$$

The material parameters assumed in this case are shown in Table 9 for the Ogden material and $C_{10} = 2.1125 \times 10^6$ N/m^2 for the Neo-Hookean material. The ratio of initial shear moduli of fiber and matrix is 6.8.

A simple transverse shear strain is imposed to the UC, with a deformation gradient as studied in the previous case (Eq. (44)). Eq. (35) was used to evaluate Cauchy stress. Results of the present post-processing model are compared in Fig. 7 with those obtained by numerical integration of Eq. (4), and excellent agreement is found between them.

4. Results for UC under a uniaxial state

4.1. Comparison with an analytical model under finite strains

Results obtained by the rule of mixtures (ROM) are compared in this section with the present PPM-FS. Based on a thermodynamical formulation, the ROM allows writing the macroscopic stress tensor of a composite formed by N constituent materials at the micro scale as

$$\sigma = \sum_{i=1}^{N} V f_i \sigma_i \tag{54}$$

where Vf_i is the volume fraction for each constituent; and $\boldsymbol{\sigma}_i$ is the stress tensor in the ith microstructural component. Eq. (54) can be used for heterogeneous materials with arbitrary constitutive laws at the micro scale (Martínez and Oller, 2009), and is a good approximation for long fiber composites.

To illustrate the behavior, a prismatic UC with a square fiber arrangement ($\theta = 90$ in Fig. 2a) is considered under uniaxial state, as given by Eq. (25). Fiber and matrix are assumed as hyper-elastic with material properties given in Section 3.3. Eq. (32) was used to perform homogenization.

For this composite, Eq. (54) is given by

$$\sigma_{11} = v_f \sigma_f + (1 - v_f)\sigma_m \tag{55}$$

in direction of the fiber, where σ_f and σ_m are Cauchy normal stresses in the fiber direction, acting on the fiber and matrix, respectively. Such stresses are next obtained from hyper-elastic models and the imposed strain.

The strain energy density can be evaluated by using Eq. (40), i.e.

$$W = C_{10}(I_1 - 3) \tag{56}$$

The deformation gradient for a uniaxial stress state (in which $\sigma_{22} = \sigma_{33} = 0$) in an incompressible material is

$$\mathbf{F} = \begin{bmatrix} \lambda_1 & 0 & 0 \\ 0 & \lambda_1^{-\frac{1}{2}} & 0 \\ 0 & 0 & \lambda_1^{-\frac{1}{2}} \end{bmatrix} \tag{57}$$

Notice that $J = \det(\mathbf{F}) = 1$, so that the first strain invariant I_1 is

$$I_1 = \mathrm{tr}\left[\mathbf{F}^T\mathbf{F}\right] \quad \text{or} \quad I_1 = \lambda_1^2 + \frac{2}{\lambda_1} \tag{58}$$

Substitution into (56) yields

$$W = C_{10}\left(\lambda_1^2 + \frac{2}{\lambda_1} - 3\right) \tag{59}$$

In an hyper-elastic model in which W is written in terms of principal stretching (λ_{ii}), Cauchy principal stresses may be obtained as (Eq. 6.45 in Holzapfel, 2000)

$$\sigma_a = J^{-1}\lambda_a \frac{\partial W}{\partial \lambda_a} \tag{60}$$

Finally, the fiber stress is

$$\sigma_f = 2\lambda_1 C_{10}\left(\lambda_1 - \frac{1}{\lambda_1^2}\right) \tag{61}$$

The same procedure is used for the matrix following Ogden's model:

$$W = \sum_{i=1}^{3} \frac{2\mu_i}{\alpha_i^2}\left[\lambda_1^{\alpha_i} + \lambda_2^{\alpha_i} + \lambda_3^{\alpha_i} - 3\right] \tag{62}$$

which, under uniaxial strain, reduces to

$$W = \sum_{i=1}^{3} \frac{2\mu_i}{\alpha_i^2}\left[\lambda_1^{\alpha_i} + 2\lambda_1^{-\frac{\alpha_i}{2}} - 3\right] \tag{63}$$

Considering Eqs. (60) and (63), Cauchy stress for the matrix is

$$\sigma_m = \sum_{i=1}^{3} \frac{2\mu_i}{\alpha_i}\left[\lambda_1^{\alpha_i} - \lambda_1^{-\frac{\alpha_i}{2}}\right] \tag{64}$$

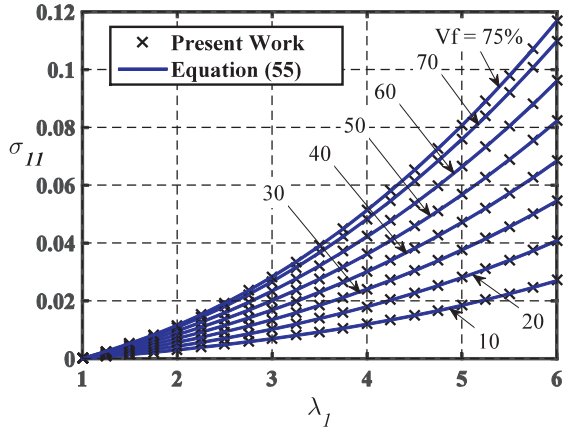

Fig. 8. Cauchy stress [GPa] for a hyper-elastic composite under uniaxial stress state: Comparison between PPM-FS and Eq. (55).

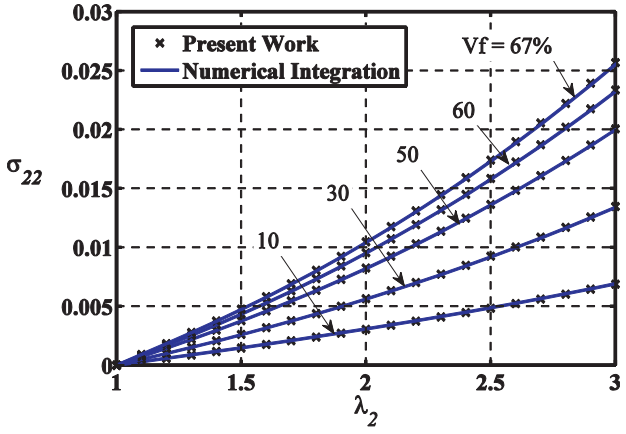

Fig. 9. Cauchy stress [GPa] for a hyper-elastic composite under uniaxial stress state: Comparison between PPM-FS and numerical integration of Eq. (4).

The analytical model used in this section to validate PPM-FS, described in Eq. (55), is now complete with fiber and matrix stresses as given by Eqs. (61) and (64). Stress results, computed by Eqs. (32) and (55), for $0.1 \leq Vf \leq 0.75$, are shown in Fig. 8. Excellent agreement is found between both models.

4.2. Comparison with a numerically integrated model for finite strains

Numerical integration of Eq. (4) has been performed in this case under a transverse uniaxial state in direction 2. In this case

$$\mathbf{F}(t) = \begin{bmatrix} \lambda_1(t) & 0 & 0 \\ 0 & \lambda_2(t) & 0 \\ 0 & 0 & \lambda_3(t) \end{bmatrix} \tag{65}$$

where λ_2 is imposed and λ_1 and λ_3 are evaluated using $\sigma_{11} = \sigma_{33} = 0$, so that a uniaxial stress state exists in direction 2. The material properties and hexagonal fiber arrangement (prismatic UC with $\theta = 60$ in Fig. 2a) are assumed as in Section 3.3. Cauchy stress was evaluated by means of Eq. (36).

Results of σ_{22} from numerically integrated and PPM-FS are shown in Fig. 9 for values of the imposed deformation gradient component $F_{22} = \lambda_2$. Again, almost identical results are obtained using both methods.

4.3. Problems in which there is contact within the RVE

A composite with interface damage around the complete fiber is investigated in this section. Interest in this case occurs because

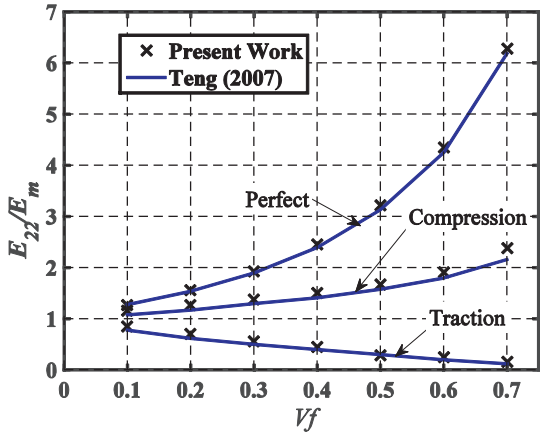

Fig. 10. Normalized transversal modulus of elasticity E_{22} as a function of fiber volume fraction *Vf*. Results for a perfectly bounded and a completely debonded fiber, under uniaxial transverse tensile and compressive states.

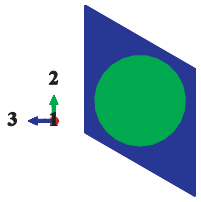

Fig. 11. Fiber reinforced composite with hexagonal arrangement.

tensile stresses normal to the interface generate separation between materials; but if compression occurs at the interface there is load transfer between them because materials cannot penetrate each other (Teng, 2007). In a composite with interface damage, the material has different elasticity modules in tension and compression (bi-modular behavior).

This problem was studied by Teng (2007) for a composite with fibers having $0.1 \leq Vf \leq 0.7$, using a square configuration with 10×10 fibers. Linearly elastic and isotropic properties were assumed with $E_f = 80$ GPa, $\nu_f = 0.2$, $E_m = 4$ GPa, and $\nu_m = 0.38$; uniform tractions were applied at the boundaries, and periodicity was achieved because an extended 10×10 domain was modeled.

The PPM-FS was used on a single fiber in the UC in generalized plane strain conditions, in which a uniaxial stress in direction 2 (perpendicular to the fiber direction) is imposed. Cauchy stresses were evaluated by Eq. (36) and periodic boundary conditions were assumed. Contact in both models was assumed to occur without friction or cohesion.

Results are compared in Fig. 10 for conditions of undamaged and damaged around the fiber under uniaxial tension and compression. Very good agreement is found in all cases between the present post-processing model and the results of Teng (2007), with minor discrepancies caused by differences in the boundary conditions assumed in each case.

4.4. Problems involving plasticity

Michel et al. (1999) considered plasticity for Cauchy stress at the macro level in direction 3 perpendicular to the fiber direction, in a composite with hexagonal fiber configuration, as shown in Fig. 11. Elastic-perfectly plastic properties were assumed with $E^m = E^f = 100$ GPa, $\nu^m = \nu^f = 0.25$; von Mises plasticity with an associative rule were used, with ${\sigma_0}^m = 100$ MPa and ${\sigma_0}^f = 500$ MPa. Fiber volume fraction of 56.25% was assumed in a prismatic UC.

In modeling this case, Eq. (36) is used for homogenization. A strain due to a uniaxial stress state in direction 3 is assumed so

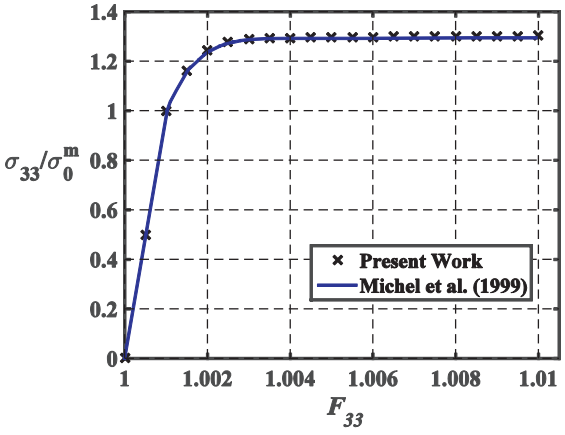

Fig. 12. Normalized Cauchy stress in direction 3. Results of PPM-FS and Michel et al. (1999) for an elastic perfectly-plastic composite.

that the imposed deformation gradient is given by Eq. (25). In a way similar to other uniaxial cases considered previously in this paper, λ_3 is imposed and λ_1 and λ_2 are calculated to have zero normal stresses in directions 1 and 2.

Results from Michel et al. (1999) are compared with the present PPM-FS in Fig. 12, to show that even for cases involving plasticity there is an excellent performance by use of the post-processing methodology.

5. Conclusions

A new post-processing methodology has been presented in this work to evaluate stresses at the macro level in computational micro-mechanics. The procedure can be used in finite strain as well as in cases in which there is plasticity, and is limited to quasi-static cases. The formulation accounts for uniaxial load and shear.

The methodology greatly simplifies evaluation of stresses at the macro level because numerical integration in the RVE domains is not performed; this avoids complexities in implementation. Further, the present procedure allows having a unified treatment of problems that were before considered with specific or ad-hoc methodologies.

Validation has been presented by comparison with independent cases solved in the literature (either analytical or numerical) to evaluate elastic properties of linearly elastic composites in a truncated octahedron UC domain under small strains; elastic properties of composites in which there is contact at the fiber/matrix interface; stresses at the macro scale considering plasticity, and hyperelasticity under finite strains.

Because the present formulation was derived from Hill-Mandel principle, the approach is not limited to periodic conditions in the RVE, and could also be employed for other boundary conditions which could be implemented by means of control nodes, such as linear boundary conditions.

Some limitations in the present formulation should be mentioned: It is valid in cases in which an effective constitutive tensor is pursued. On the other hand, the methodology is not appropriate if averaged macro-stress must be solved in each time step, i.e. in a problem subjected to a loading process.

Acknowledgments

NDB and LAG were supported by CONICET, the Science Research Council of Argentina during this research. The authors thank the support received from grants of CONICET (PIP 0126), SECyT-UNC, Ministerio de Ciencia y Tecnología de la Prov. de Córdoba, and UTN-FRC (UTI 2119).

References

Abadi, M.T., 2010. Characterization of heterogeneous materials under shear loading at finite strain. Compos. Struct. 92 (2), 578–584. doi:10.1016/j.compstruct.2009.09.002.

Abaqus v. 6.7, 2009. Dassault SystÃ¨mes, Providence, RI, USA.

Barbero, E.J., 2013. Finite Element Analysis of Composite Materials Using Abaqus TM. CRC Press, Boca Ratón.

Chandrasekharaiah, D.S., Debnath, L., 2014. Continuum Mechanics. Elsevier.

de Souza-Neto, E.A., Feijóo, R.A., 2008. On the equivalence between spatial and material volume averaging of stress in large strain multi-scale solid constitutive models. Mech. Mater. 40 (10), 803–811. doi:10.1016/j.mechmat.2008.04.006.

de Souza-Neto, E.A., Blanco, P.J., Sánchez, P.J., Feijóo, R.A., 2015. An RVE-based multiscale theory of solids with micro-scale inertia and body force effects. Mech. Mater. 80, 136–144. doi:10.1016/j.mechmat.2014.10.007.

Delannay, L., Jacques, P.J., Kalidindi, S.R., 2006. Finite element modeling of crystal plasticity with grains shaped as truncated octahedrons. Int. J. Plast. 22 (10), 1879–1898. doi:10.1016/j.ijplas.2006.01.008.

Dijk, N.P., 2015. Formulation and implementation of stress-driven and/or strain-driven computational homogenization for finite strain. Int. J. Numer. Methods Eng. doi:10.1002/nme.5198.

Dharmasena, K.P., Wadley, H.N.G., 2002. Electrical conductivity of open-cell metal foams. J. Mater. Res. 17 (03), 625–631. doi:10.1557/JMR.2002.0089.

Guo, Z., Peng, X., Moran, B., 2007. Large deformation response of a hyperelastic fibre reinforced composite: Theoretical model and numerical validation. Compos. Part A 38 (8), 1842–1851. doi:10.1016/j.compositesa.2007.04.004.

Guo, Z., Shi, X., Chen, Y., Chen, H., Peng, X., Harrison, P., 2014. Mechanical modeling of incompressible particle-reinforced neo-Hookean composites based on numerical homogenization. Mech. Mater. 70, 1–17. doi:10.1016/j.mechmat.2013.11.004.

Holzapfel, G.A., 2000. Nonlinear Solid Mechanics, Vol. 24. Wiley, Chichester.

Li, S., Wongsto, A., 2004. Unit cells for micromechanical analyses of particle-reinforced composites. Mech. Mater. 36 (7), 543–572. doi:10.1016/S0167-6636(03)00062-0.

Martínez, X., Oller, S., 2009. Numerical simulation of matrix reinforced composite materials subjected to compression loads. Arch. Comput. Methods Eng. 16 (4), 357–397. doi:10.1007/s11831-009-9036-3.

Michel, J.C., Moulinec, H., Suquet, P., 1999. Effective properties of composite materials with periodic microstructure: a computational approach. Comput. Methods Appl. Mech. Eng. 172 (1), 109–143. doi:10.1016/S0045-7825(98)00227-8.

Nemat-Nasser, S., Hori, M., 1999. Micromechanics: Overall Properties of Heterogeneous Materials. Elsevier, North-Holland, Amsterdam.

Oller, S., Miquel-Canet, J., Zalamea, F., 2005. Composite material behavior using a homogenization double scale method. J. Eng. Mech. 131 (1), 65–79. doi:10.1061/(ASCE)0733-9399(2005)131:1(65).

Sun, C.T., Vaidya, R.S., 1996. Prediction of composite properties from a representative volume element. Compos. Sci. Technol. 56 (2), 171–179. doi:10.1016/0266-3538(95)00141-7.

Teng, H., 2007. Transverse stiffness properties of unidirectional fiber composites containing debonded fibers. Compos. Part A 38 (3), 682–690. doi:10.1016/j.compositesa.2006.10.002.

Zahr-Viñuela, J., Pérez-Castellanos, J., 2011. Elastic constants and isotropy considerations for Particulate Metal-Matrix Composites. A multi-particle, cell-based approach. Compos. Part A 42 (5), 521–533. doi:10.1016/j.compositesa.2011.01.011.

Zohdi, T.I., Wriggers, P., 2008. An Introduction to Computational Micromechanics. Springer.